

DRAM Failure Analysis with the Force-Based Scanning Kelvin Probe

Todd Hochwitz, Albert K. Henning, and Charles Daghlian
Dartmouth College
Hanover, NH 03755

Ronald Bolam, Peter Coutu, Robert Gluck, and James Slinkman
IBM Microelectronics
Essex Junction, VT 05452

Abstract — A fabrication induced failure in complementary metal-oxide-semiconductor dynamic random access memory (CMOS DRAM) cells has been imaged successfully with a novel combination of atomic force and scanning Kelvin probe microscopes. The imaging system was used to verify the presence, and subsequent removal of, ionic contaminants on a sub-micron scale.

INTRODUCTION

A novel combination of atomic force (AFM) and scanning Kelvin probe microscope (SKPM) has been used to examine fabrication related defects in integrated circuits on a sub-micron scale [1–3]. In this study, the force-based SKPM has been used to aid in the verification of the nature of a failure mechanism in DRAM cells.

The SKPM was chosen as an analysis tool for several reasons. The technique is non-destructive and minimally invasive, allowing us to image the failure mechanisms without disturbing the devices. In addition, a probing pad is not required because the non-contact nature of the measurement system enables investigation of the electrical properties of RAM cells in the middle of arrays. Lastly, the instrument provides simultaneous information about the topography, material, and capacitive properties of the sample under study.

The remainder of this document will be used to describe the operational aspects of the force-based SKPM, the electrical failure of the DRAM cell, and results of the measurements made with the SKPM. The use of these measurements in changing the fabrication process for successful removal of the cause for the failure will be described in the conclusion, along with plans for future research.

SYSTEM OPERATION

Our force-based SKPM is based upon a non-contact AFM originally built at IBM's Thomas J. Watson Research Center [4]. We have added the necessary electronics to convert the system to the force-based SKPM [5]. Figure 1 shows a block diagram of the microscope. The sample remains stationary, while a set of piezo stacks and mechanical levers (Piezo Flex stage [6]) is used to adjust the lateral position of either a silicon [7] or tungsten probe over a sample with a 100 μm range

and 1 nm positionability. A heterodyne interferometer is used to determine the deflection of the probe due to the atomic scale forces.

There are two control loops in the feedback which are used to make the measurements. For one control loop the probe is oscillated mechanically with a piezoelectric bimorph at a frequency slightly higher than the dominant mechanical resonant frequency of the probe. Changes in the amplitude of oscillation at this frequency are used to adjust the spacing between the probe and sample to maintain a constant van der Waals (vdW) force gradient. This yields an approximation of the surface topography. The other control loop is used to make measurements of the electrical properties of the sample under the probe.

The mechanical deflection of a cantilever due to an electrostatic force between the probe and sample has been examined by several researchers and treated as a capacitive system [8–11]. The force on the probe due to a potential difference between the probe and sample may be represented as [12]:

$$F_e = -\frac{1}{2}V^2C' \quad (1)$$

$$C' = \left(\frac{C_{\text{eff}}}{C_{\text{air}}}\right)^2 \frac{\partial C_{\text{air}}}{\partial z} \quad (2)$$

where V is the total potential difference, z is the spatial distance, C_{air} is the effective capacitance and $\frac{\partial C_{\text{air}}}{\partial z}$ is the spatial derivative of the effective capacitance between the probe and sample, and C_{eff} is the total capacitance in series with the system (including C_{air}). Theoretical analysis indicates that the amount of cantilever deflection is directly proportional to the magnitude of this force [13]. Thus, variations in the electrical nature of the probe/sample system can be examined by detecting and properly correcting for changes in the mechanical deflection of the cantilever.

With the SKPM the potential difference V consists of one dc component and one ac component, which may be represented as follows:

$$V = V(t) = V_{DC} - \frac{\Delta\Phi}{q} + V_{ac} \sin(\omega t) \quad (3)$$

where V_{DC} is the magnitude of the dc component applied by any external electronics, $\Delta\Phi$ is the work function differ-

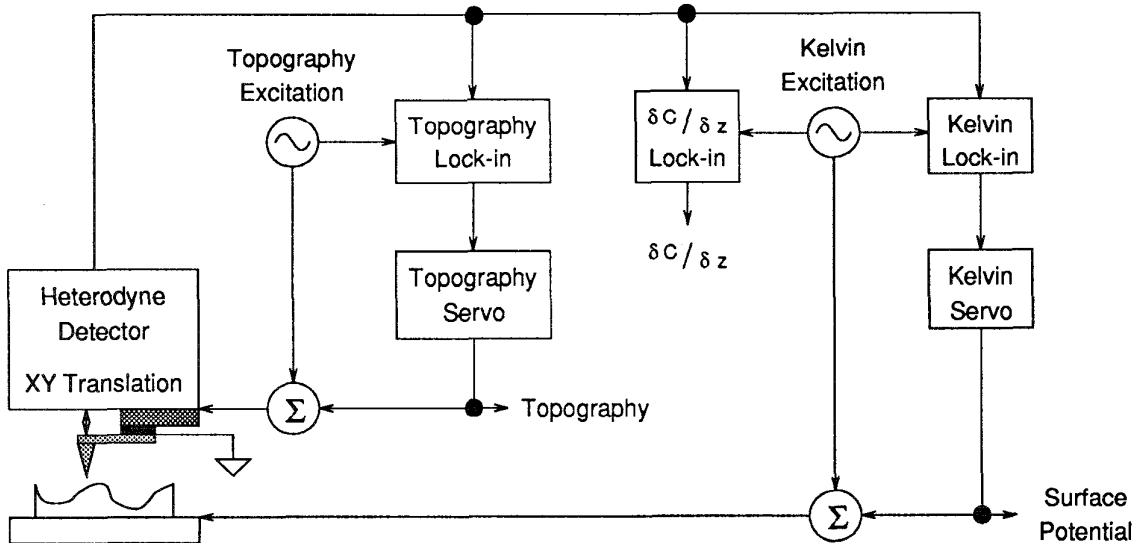


Figure 1: Block diagram of the force-based scanning Kelvin probe microscope.

ence (WFD) (in eV) of the materials, V_{ac} is the peak magnitude of the ac component of the externally applied potential between the probe and the sample, and ω is the frequency at which the ac voltage is oscillating.

If V in Equation 1 is replaced by the form given in Equation 3 and expanded, one obtains a force that consists of three components:

$$F_e = \frac{1}{2} \left(\left(V_{DC} - \frac{\Delta\Phi}{q} \right)^2 + \frac{1}{2} V_{ac}^2 \right) C' \quad (4)$$

$$+ C' \left(V_{DC} - \frac{\Delta\Phi}{q} \right) V_{ac} \sin(\omega t) \quad (5)$$

$$+ \frac{1}{4} C' V_{ac}^2 \cos(2\omega t) \quad (6)$$

Note that the negative sign from Equation 1 has been removed since the mechanical deflection of the cantilever is proportional to the magnitude of the force. An interferometer is used to monitor deflections at the frequencies of ω and 2ω . The deflection at 2ω , which is proportional to Equation 6, will yield capacitance information about the sample. In this document the images obtained from this signal are designated as C' . The signal detected at ω , which is proportional to Equation 5, is used to minimize the electrostatic force. Since the capacitive and ac terms of Equation 5 are non-zero, the primary method to minimize the deflection of the cantilever at ω is to adjust V_{DC} until it is equal to the WFD between the sample and the probe.

This assumes that all of the force is sensed only between the tip of the probe and the surface of the sample. There is significant coupling between the sample and the cantilever of the silicon probes that we typically use [14]. Thus, the dc voltage needed to minimize the signal at ω is not equal to the exact WFD between the probe and sample. It is dependent upon contributions from materials a short distance from the

area under investigation, and leads to measured WFDs that are smaller than theoretical values. The data obtained is therefore qualitative in nature, and to obtain quantitative information requires deconvolution of the measurements. Since the feedback voltage of V_{DC} is not exactly the true WFD, we refer to the raw data as an electrochemical potential difference (EPD) image rather than a WFD image.

The feedback voltages from the vdW and EPD loops, and the magnitude of the capacitive signal, are collected with a computer via an analog-to-digital converter board. We then use the collected data to generate 2D surfaces, 1D line profiles, or grey-scale images of the measurements for further analysis and processing.

The system consistently achieves lateral resolutions under 100 nm, a closed loop vdW noise level of $0.5 \text{ \AA}/\sqrt{\text{Hz}}$ measured in a 100 Hz bandwidth, and a closed loop EPD noise level of $5 \text{ mV}/\sqrt{\text{Hz}}$ measured in a 160 Hz bandwidth. The system has achieved lateral resolutions of 25 nm, a closed loop vdW noise level of $0.1 \text{ \AA}/\sqrt{\text{Hz}}$, and a closed loop EPD noise level of $1 \text{ mV}/\sqrt{\text{Hz}}$.

Successful measurements have been taken with this system on samples prepared under a variety of conditions, from cleaning the surface with compressed air to buffered HF dips. Measurement times are dependent upon the desired resolution and scan size. The majority of the scans shown in this manuscript took 15 to 20 minutes to generate. Measurements have been shown to be reproducible over a 2 month period of time.

FAILURE DESCRIPTION

The electrical failure in the device discussed in this manuscript occurred in a structure near the edge of the RAM array. Extensive electrical measurements were made by the

Failure Analysis group at IBM – Essex Junction. During testing, it was discovered that charge was leaking out of the storage cell. The electrical measurements ruled out problems with dopants, since the devices were otherwise functioning as designed. The measurements also indicated that the charge was being bled off between devices, and not leaking through the substrate.

These failure signatures were similar to those seen in earlier technologies. They were indicative of ionic contaminants in the region near the dielectric of the storage trench, which caused neighboring transistors to turn on slightly and allowed charge to bleed off. However, no direct evidence supported this mechanism. The SKPM was used in an attempt to image the presence of any ionics in the region of a failing device.

DRAM MEASUREMENTS

The sample was prepared at IBM – Essex Junction and scanned with the SKPM at Dartmouth College. The preparation consisted of a mechanical polish to remove upper levels of circuitry and dielectric material, followed by an etch to remove the word lines from the memory array. The sample was then cleaned with de-ionized (DI) water, air dried, mounted on a holder, and scanned with the SKPM.

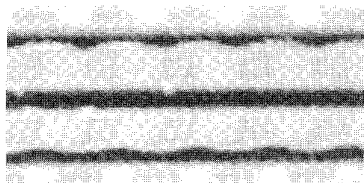


Figure 2: vdW image showing the topography of the sample surface in the area of the failing device. The scan was made prior to bake. The brightest features along the top and bottom are metal contacts, gray indicates oxide, and the dark horizontal stripes are remnants of the word lines. The failing device is in the center of this and all subsequent images.

Figure 2 shows the vdW image from an initial scan of the sample. The image indicates the presence of some foreign material near the edge of the oxide regions, but no significant surface defects are seen that would be responsible for the electrical failure.

Based upon the performance of the microscope, we suspect there was a thin layer of surface moisture on the sample from the DI water. In comparing Figures 2 and 6, the edges of the oxide clearly show a difference in the response of the vdW control loop.

The impact of surface moisture upon the measurements must be considered. If the moisture is distributed uniformly, it will behave as an extra dielectric layer between the probe and sample electrodes. In this case, any contrast detected in

either the C' or EPD images will be due to material differences between the RAM cells and not the variations in the surface moisture. In terms of qualitative analysis the moisture may be ignored as long as it doesn't influence the tracking of the vdW control loop. For quantitative data analysis it would be necessary to include the presence of the moisture.

The fluctuations are seen in the vdW signal of Figure 2 only near the edges of structures, whereas along the oxide surface the water did not appear to affect the vdW feedback. It did appear to have an effect upon the EPD signal due to the technique's sensitivity to surface conditions. More features were resolved after the water was removed, and the contrast of the metal contacts was inverted. The C' signal remained consistent prior to and after the bake due to its sensitivity to the entire electrical path between the electrodes. As long as the analysis is restricted to the oxide and word line regions, and not applied to the edges of the oxide layers, we can make a direct qualitative comparison between the scans prior to and after the baking process.

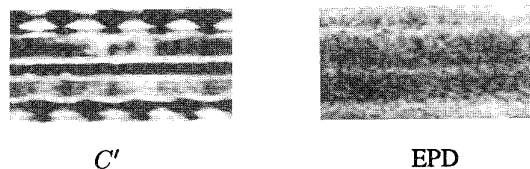


Figure 3: Electrical measurements of the fail area prior to bake. The Kelvin loop was run with an applied $V_{ac} = 2$ Volts. The metal contacts from Figure 2 appear here as dark features in the C' image and as lighter features in the EPD image.

Figure 3 shows the electrical measurements from the SKPM with an applied $V_{ac} = 2$ Volts. The EPD signal does not show significant contrast between different RAM cells, indicating that the devices are similar – at least near the surface. The C' signal clearly shows a very significant contrast change in the area surrounding the failing device. The contrast is seen in the partial shape of the storage trench. This contrast indicates the defect lies near the dielectric material of the trench, supporting the theorized failure mechanism described in the previous section.

Interestingly, the contrast appears to have a gap where the word line had been present. We believe this is due to the interaction between the cantilever and the surface. As mentioned in an earlier section, we have noted significant interaction between the cantilever of our silicon probes and the sample surface, which leads to signal reduction. As the probe scans the word line regions, the cantilever/sample distance decreases, which leads to an increased capacitive coupling relative to the tip/sample capacitance. The feature imaged in Figure 3 is probably also present in the area of the word line, but would require deconvolution of the data in order to resolve it.

Figure 4 shows the electrical measurements from the SKPM with an applied $V_{ac} = 0.5$ Volts. During this scan, the tip of the probe charged slightly while over the top oxide section. In this case, the EPD becomes a mixture of WFD and C'

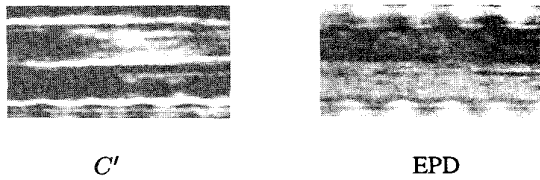


Figure 4: Electrical measurements in the fail area prior to bake with an applied $V_{ac} = 0.5$ Volts.

variations, with the defect area seen as a slight change in the contrast consistent with the C' image. A much smaller defect has been imaged in the C' signal. Since the magnitude of V_{ac} has decreased, the energy bands are changed by a smaller amount, localizing any mobile ionic charge. The defect site appears in the upper right section of the storage trench, roughly in the middle of the defect area imaged in Figure 3, showing consistency in the measurements.

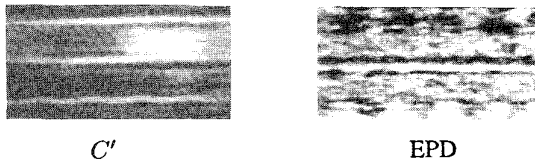


Figure 5: Electrical measurements in the fail area prior to bake with an applied $V_{ac} = 0.2$ Volts.

Figure 5 shows the electrical measurements from the SKPM with an applied $V_{ac} = 0.2$ Volts. The level of V_{ac} is starting to reach the lower limits for detection, so the EPD contrast is significantly reduced. But as in Figures 3 and 4, no difference is seen between the RAM cells. Consistent with the previous scans, the C' signal clearly shows the defect in an even smaller area. The feature is seen to be localized to the upper right section of the storage cell.

After these initial scans, the sample was placed in an oven and baked for two hours at 350°C . If ionic contaminants were in fact being imaged, the baking process would mobilize and dissipate them. Further imaging with the SKPM should then detect no contrast in the area of the failing device. The baking process would also remove the surface moisture that appeared to be on the sample surface.

Figure 6 shows the vdW image from a scan of the sample after bake. As discussed earlier, the signal is much cleaner, which we attribute to removal of surface moisture. There is no discernible difference between the topography pre- and post-bake, which means the physical surface of the sample was unaltered. Therefore, any changes from the previous scans are due to changes in the electrical properties of the materials.

Electrical measurements were made under the same bias conditions as the scans prior to the bake. The contrast in the C' signal did not change from the previous set of scans. However, the contrast of the EPD signal over the metal contact lines did change, which is not completely understood at this time. It is likely due to the interaction of the metal surface with the moisture that had been present during the initial set of

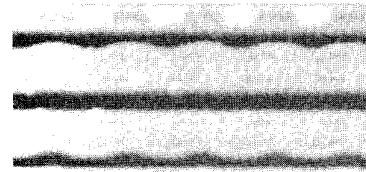


Figure 6: vdW image showing the topography of the sample surface in the area of the failing device. The scan was post-bake. In comparison to Figure 2 the baking process did not alter the physical composition of the sample surface.

scans. The EPD signal remained consistent within the region of the RAM cells, and shows more detail due to removal of the surface moisture.

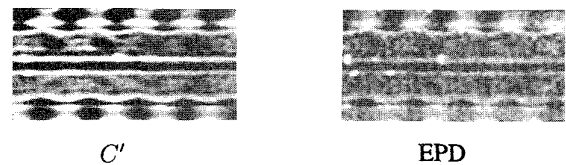


Figure 7: Electrical measurements in the fail area after bake with an applied $V_{ac} = 2$ Volts.

Figure 7 shows the electrical measurements from the SKPM with an applied $V_{ac} = 2$ Volts. As in Figure 3, the EPD signal shows no significant contrast between adjacent RAM cells. No contrast is detected in the C' signal, indicating the anomaly from the previous scans has been displaced. This result is consistent with the theory that ionics were present in dielectric material, were driven out by the baking process.



Figure 8: Electrical measurements in the fail area after bake with an applied $V_{ac} = 0.5$ Volts.

Figures 8 and 9 show the electrical measurements made with a bias of $V_{ac} = 0.5$ Volts and $V_{ac} = 0.2$ Volts, respectively. Once again, the EPD images indicate no changes near the surface of the devices under examination. The contrast detected in the C' images of Figures 3 through 5 has disappeared.

CONCLUSION

The SKPM measurements support strongly the theory that

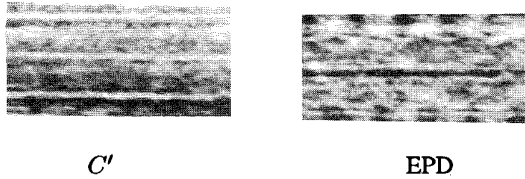


Figure 9: Electrical measurements in the fail area after bake with an applied $V_{ac} = 0.2$ Volts.

the failure mechanism in the RAM cell was the presence of ionic contaminants in the dielectric material near the storage trench. Electrical measurements on the sample after scanning with the SKPM would be needed to confirm that the disappearance of the anomalous feature restored proper device function.

Unfortunately, this verification was not possible due to the removal of the word lines during sample prep. Instead, a second failing sample was put through a similar baking process and tested electrically. In that sample the devices functioned post-bake. We therefore conclude that the SKPM imaged the suspected failure mechanism in these devices successfully.

Tests at IBM were able to induce the failure in other RAM cells. As a result of the SKPM, electrical, and stressing measurements, the fabrication process was changed successfully to remove the failure mechanism from later batches of memory chips. The ionic contamination was induced by the presence of nitride in the dielectric material. The nitride stress caused the material energy bands to shift by amounts large enough to generate a significant internal electric field. This strong electric field trapped ions during the fabrication process. Removal of nitride from the area resulted in less stress, and hence the disappearance of the failure.

These results, in addition to measurements from other devices of technological interest [1–3], indicate that the SKPM is a viable tool for use in failure analysis. The functionality of a force-based SKPM may be added to any non-contact AFM at minimal cost, and the measurements may be performed in a lab or fabrication line environment. Sample preparation can be minimal, although standard cleaning procedures will likely be necessary for successful quantitative results.

The technique has a lateral resolution well into the sub-micron range, and is sensitive to electrical signatures on the milli-Volt level. The small probe size and non-contact nature of the technique allow us to obtain electrical measurements without the need for large probing pads or the use of FIB tools to alter the device structure. Results to date have been qualitative in nature. Research is underway to reach a better understanding of the nature of the electrostatic force leading to a robust technique for extraction of quantitative information from measurement data.

ACKNOWLEDGMENTS

The authors acknowledge the following sources with gratitude: P. Cadrecha and the management of IBM – Essex Junction for equipment and personnel support; research support (for TH and AKH) through an IBM Shared University Re-

search Grant, an Analog Devices Career Development Professorship, and Thayer School of Engineering funds; and M. O’Boyle for his aid in adding the Kelvin capabilities to the AFM. This manuscript was prepared using L^AT_EX [15] and dvips [16]. Figures were generated with xfig [17] and NetPBM [18].

REFERENCES

- [1] T. Hochwitz, A. K. Henning, C. Levey, C. Daghljan, J. Slinkman, J. Never, P. Kaszuba, R. Gluck, S. Hoffmann, and M. O’Boyle, “Failure analysis using scanning Kelvin probe microscopy,” in *1994 Fall Meeting of the IBM Failure Analysis Technical Exchange*, 1994.
- [2] T. Hochwitz, A. K. Henning, C. Levey, C. Daghljan, J. Slinkman, J. Never, P. Kaszuba, R. Gluck, R. Wells, J. Pekarik, and R. Finch, “Imaging integrated circuit dopant profiles with the force-based scanning Kelvin probe microscope,” in *Proceedings of the Third Intl. Workshop on the Measurement and Characterization of Ultra-Shallow Doping Profiles in Semiconductors*, 1995.
- [3] Martin O’Boyle and Tom Hwang, private discussions.
- [4] Y. Martin, C. C. Williams, and H. K. Wickramasinghe, “Atomic force microscope-force mapping and profiling on a sub 100 Å scale,” *J. Appl. Phys.*, vol. 61, pp. 4723–4729, (1987).
- [5] M. Nonnenmacher, M. P. O’Boyle, and H. K. Wickramasinghe, “Kelvin probe force microscopy,” *Appl. Phys. Lett.*, vol. 58, pp. 2921–2923, (1991).
- [6] Wye Creek Instruments, 10809 Gambrill Park Road Frederick, MD 21701.
- [7] O. Wolter, Th. Bayer, and J. Greschner, “Micromachined silicon sensors for scanning force microscopy,” *J. Vac. Sci. Technol. B*, vol. 9, pp. 1353–1357, (1991).
- [8] G. M. McClelland, R. Erlandsson, and S. Chiang, “Atomic force microscopy: General principles and a new implementation,” in D. O. Thompson and D. E. Chimenti, editors, *Review of Progress in Quantitative Nondestructive Evaluation*. New York: Plenum, 1987, page 1307.
- [9] Y. Martin, D. W. Abraham, and H. K. Wickramasinghe, “High-resolution capacitance measurement and potentiometry by force microscopy,” *Appl. Phys. Lett.*, vol. 52, pp. 1103–1105, (1988).
- [10] H. W. Hao, A. M. Baró, and J. J. Sáenz, “Electrostatic and contact forces in force microscopy,” *J. Vac. Sci. Technol. B*, vol. 9, pp. 1323–1328, (1991).
- [11] D. Sarid, *Scanning Force Microscopy with Applications to Electric, Magnetic, and Atomic Forces*. New York: Oxford University Press, 1991.
- [12] D. W. Abraham, C. C. Williams, J. Slinkman, and H. K. Wickramasinghe, “Lateral dopant profiling in semiconductors by force microscopy using capacitive detection,” *J. Vac. Sci. Technol. B*, vol. 9, pp. 703–706, (1991).
- [13] D. Sarid and V. Elings, “Review of scanning force microscopy,” *J. Vac. Sci. Technol. B*, vol. 9, pp. 431–437, (1991).

- [14] T. Hochwitz, A. K. Henning, C. Levey, C. Daghljan, and J. Slinkman, "Capacitive effects on quantitative dopant profiling with scanned electrostatic force microscopes," in *Proceedings of the Third Intl. Workshop on the Measurement and Characterization of Ultra-Shallow Doping Profiles in Semiconductors*, 1995.
- [15] \TeX by D. Knuth and \LaTeX by L. Lamport. Available via anonymous ftp from one of the Comprehensive \TeX Archive Network (CTAN) sites: ftp.dante.de (Internet address 129.206.100.192), ftp.tex.ac.uk (Internet address 134.151.44.19), and pip.shsu.edu (Internet address 192.92.115.10).
- [16] T. Rokicki, Radical Eye Software. Available via anonymous ftp from labrea.stanford.edu (Internet address 36.8.0.112) or one of the CTAN sites.
- [17] Originally written by K. Yap, current version maintained by B. Smith, with contributions from many authors. TransFig is written by M. Bica, with contributions from many authors. Available via anonymous ftp from ftp.cs.cornell.edu (Internet address 128.84.218.75).
- [18] NetPBM is an extension of Pbmplus (written by J. Poskanzer), with contributions from many authors. Available via anonymous ftp from wuarchive.wustl.edu (Internet address 128.252.135.4).